CrossMark

Temperature dependent photoluminescence from WS$_2$ nanostructures

Shivani Sharma[1] · Shubham Bhagat[1] · Jasvir Singh[1] · Manzoor Ahmad[2] · Sandeep Sharma[1] (ORCID)

Abstract
Owing to their intriguing physical properties, two-dimensional transition metal dichalcogenides such as WS$_2$ and MoS$_2$ have gained significant attention in the research community. Their tunable bandgap justify their use in future optical and nano-electronics devices. Here, we report the room temperature Raman spectra and temperature dependent photoluminescence of WS$_2$ nanostructures prepared in liquid media. The resonance Raman spectra revealed various first order modes together with higher order modes that were inaccessible with excitation away from resonance absorption. The luminescence from these nanostructures displayed red-shift and linear temperature dependence in the range 293–363 K. The observed negative temperature coefficients are very small and may arise from anharmonicity and thermal expansion. Further, optical measurements revealed that WS$_2$ quantum dots exhibits strong spin–orbit coupling ≈ 650 meV, larger than observed for monolayer sheets of WS$_2$ (≈ 400 meV). The stronger spin–orbit coupling together with highly luminescent nature make them attractive for applications in spintronics and optoelectronics devices.

1 Introduction

In recent few years two-dimensional materials like graphene and its inorganic analogue, i.e., transition metal di-chalcogenides (TMDCs) of type MX$_2$ (M = Mo or W and X = S, Se or Te) have attracted world-wide attention due to their intriguing physical properties and potential application in nanoelectronics and photovoltaic devices [1].Whereas graphene consist of single carbon atomic-thick layer, TMDCs (e.g. MoS$_2$, MoSe$_2$, WS$_2$, WSe$_2$, etc.), on the other hand have a "sandwich" type structure where a transition metal layer (e.g., Mo or W) is sandwiched between two chalcogen layers (e.g., S, Se or Te). As a result TMDCs are characterized by weak and noncovalent interlayer bonding similar to graphene and other van der Waals materials. This allows the exfoliation of bulk TMDCs into single or few layer sheets by various physical or chemical means including adhesive tape exfoliation [2, 3] chemical exfoliation through lithium intercalation and/or solvent assisted exfoliation [4, 5]. Another interesting feature of TMDCs is that they exhibit entirely different physical properties in monolayer or few layered form that are not seen in their bulk counterpart. This is attributed to quantum confinement and surface effects [6, 7]. For instance, in bulk form TMDCs have an indirect band gap, but when reduced to monolayers the band gap becomes direct and give rise to enhanced photoluminescence [8, 9].

Thus, tuning band gap in these 2-D materials suggest their promising use in light sensitive applications. Although band gap tuning can be achieved by various means such as induced strain in nanostructures [10] or external application of stress [11–13] doping and alloying [14]. There are other external factors which may influence the physical properties of the semiconducting materials. For instance, it is well known that optical properties in semiconductors strongly depend upon the temperature [15–17]. For instance, Pandey et al. has recently reported the existence of various optical transitions originating from excitons, biexciton and trions. Due to broad spectral features of exciton at normal temperature the experimental realization of the biexciton remains a challenging task. A systematic temperature dependent photoluminescence spectroscopy enabled them to identify various optical transitions [18]. The understanding of such optical transitions is crucial for future optoelectronic applications. Such types of systematic investigations are rare in case of WS$_2$. In view of these aspects, it is crucial to understand the response of these materials to temperature. Both micro-Raman as well as photoluminescence spectroscopy

✉ Sandeep Sharma
sandeepscl@gmail.com

1 Department of Physics, Guru Nanak Dev University, Amritsar 143005, India

2 Department of Chemistry, Guru Nanak Dev University, Amritsar 143005, India

offer a non-destructive method to characterize the structural and lattice vibrations of a crystal. Here, in this article we present room temperature Raman spectra and temperature dependent photoluminescence from WS_2 nanostructures prepared in liquid media. The emission intensity from these nanostructures decreases with rise in temperature and a weak red-shift with increasing temperature is also observed.

2 Experimental

Crystalline WS_2 powder and polyvenyle pyrrolidone (PVP) were obtained from Sigma-Aldrich and from Loba Chemie India, respectively. A mixture of 2 g WS_2 in 50 ml of deionized water together with suitable amount of PVP was processed using porbe sonicator (PCI-Analytics, India) for 1½ h. This process resulted in the exfoliation of the crystalline powder and thin sheets of WS_2 appeared on the liquid surface. These thin sheets were removed and remaining suspension was centrifuged at 12,000 rpm for 30 min. From the suspension, a few drops were transferred on glass substrates and the sample was dried in oven at 80 °C. This sample was used for Raman spectroscopy measurements. The optical characterization was performed on liquid based suspension. For transmission electron microscopy, a few drops of suspension were dropped on carbon coated copper grid. The grid was further dried under an electric bulb.

High resolution Transmission electron microscopic imaging was carried out using JEOL JEM-2100. The vibrational spectra of the WS_2 nanostructure were investigated using Renishaw Invia Reflex micro Raman spectrometer using visible excitations (488 nm and 514 nm). For investigating the optical properties of the samples, absorption spectra were recorded by using Shimadzu UV-3600 spectrophotometer. Photoluminescence study was carried out by using Fluorolog Horiba spectrometer.

3 Results and discussion

Morphology and crystal structure of the nanostructures were investigated using transmission electron microscopy. Figure 1a, b show the HR-TEM images of few layer WS_2 sheets. Sheets of different dimensions and thickness are clearly

Fig. 1 HR-TEM images for WS_2 nanostructures **a, b** shows few layer sheets of WS_2. In **b** various overlapping regions between WS_2 sheets are clearly visible. In **c** quantum dots of variable size and thickness are clearly visible. **d** Is the magnified view of quantum dots
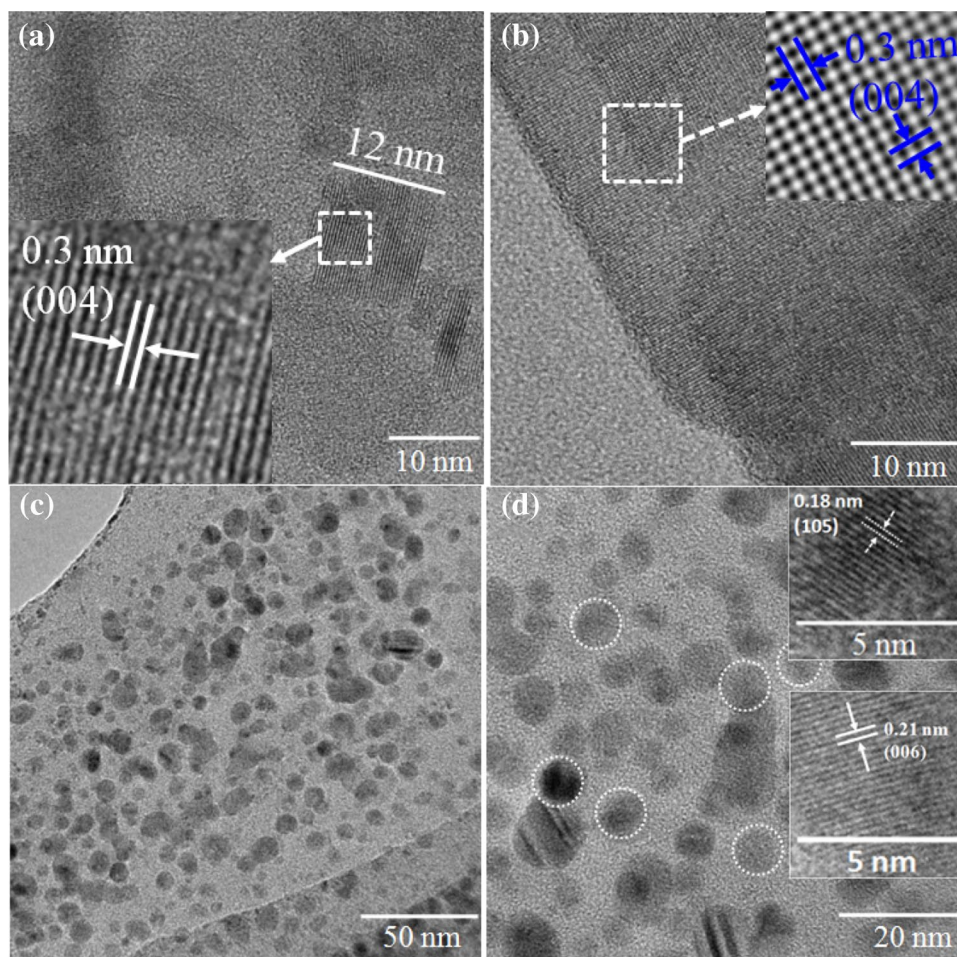
visible in the images. The image contrast in Fig. 1b implies the presence of overlapped thin sheets of WS_2. The insets in Fig. 1a, b display the digitally filtered image showing lattice fringes with 0.3 nm spacing corresponding to (004) planes. In addition to the clear planes some distortions are also visible inside the inset in Fig. 1a. This indicates that probe sonication affects the crystalline quality of the starting material. Figure 1c shows the WS_2 quantum dots of variable sizes (ranging from 4 to 10 nm). Some of the quantum dots appear to be darker as compared to other, implying the variation in the thickness also. Most of the quantum dots have size in the range of ≈ 10 nm. The insets in Fig. 1d show the HR-TEM images of the quantum dots. The fringes with interplanar spacing of 0.18 nm and 0.21 nm confirm the presence of (105) and (006) planes, respectively (JCPDS 08-0237).

Figure 2a, b display typical Raman spectra of WS_2 nanostructures acquired at room temperature using 488 nm and 514 nm excitations, respectively. With 488 nm excitation, the spectrum is dominated by two basic first order vibrational modes at the Γ point; A_{1g} (Γ) (418.1 cm^{-1}) and E_{2g}^1 (Γ) (354.14 cm^{-1}). The mode A_{ig} arises due to out-of-plane motion of the sulfur atoms whereas E_{2g}^1 originates due to relative in-plane motion of the sulfur and tungsten atoms. When compared with bulk (A_{1g} (Γ) (419.11 cm^{-1}) and E_{2g}^1 (Γ) (353.79 cm^{-1}) data not shown here) [19], the E_{2g}^1 mode is stiffened whereas A_{1g} mode is softened, possibly due to ultrathin structure of WS_2 leading to absence of layer–layer interaction [20]. It should be noted that due to ultrathin nature of the quantum dots, the relative intensity of the obtained Raman signal or peak intensity in XRD data reduce significantly [19, 20]. Broad peak at 353 cm^{-1} imply that 2LA (M) mode overlaps with E_{2g}^1 mode. In addition to these modes the spectra also contains a zone-edge mode at 175.5 cm^{-1} identified as a longitudinal acoustic mode at M point of the Brillouin zone [LA (M)] [21–23]. The multiphonon combination of these modes gives rise to additional weak peaks in the spectra. When the sample is excited at 514 nm, the Raman spectra reveals many second-order peaks relatively stronger than those observed in spectra obtained at 488 nm. The energy for excitation at 514 nm (2.41 eV) is close to the energy of the B exciton in few layer WS_2 (≈ 523 nm, 2.37 eV). Therefore, excitation at 514 nm usually gives a resonant Raman spectrum of WS_2 [22]. Thus, we see that under resonant excitation higher order Raman modes become intense. The asymmetric resonant mode at ≈ 700 cm^{-1} is assigned as 4LA(M). The mode at ≈ 580 cm^{-1} is leveled as A_{1g} (M) + LA(M), which when combined with mode A_{1g} (M) LA (M) at ≈ 233 cm^{-1} can be utilized to roughly estimate the energy of A_{1g} (M) and LA (M) modes. This gives A_{1g} (M) and LA (M) modes at 406 cm^{-1} and 176 cm^{-1}, respectively, close to experimentally observed value for LA (M) mode. Thus energy of A_{1g} (M) mode (406 cm^{-1}) is relatively farther from A_{1g} (Σ) mode (419 cm^{-1}) by 13 cm^{-1}. It is to be noted that previous reports

Fig. 2 Room temperature Raman spectra of WS_2 nanostructures obtained with an excitation wavelength **a** 488 nm, and **b** 514 nm
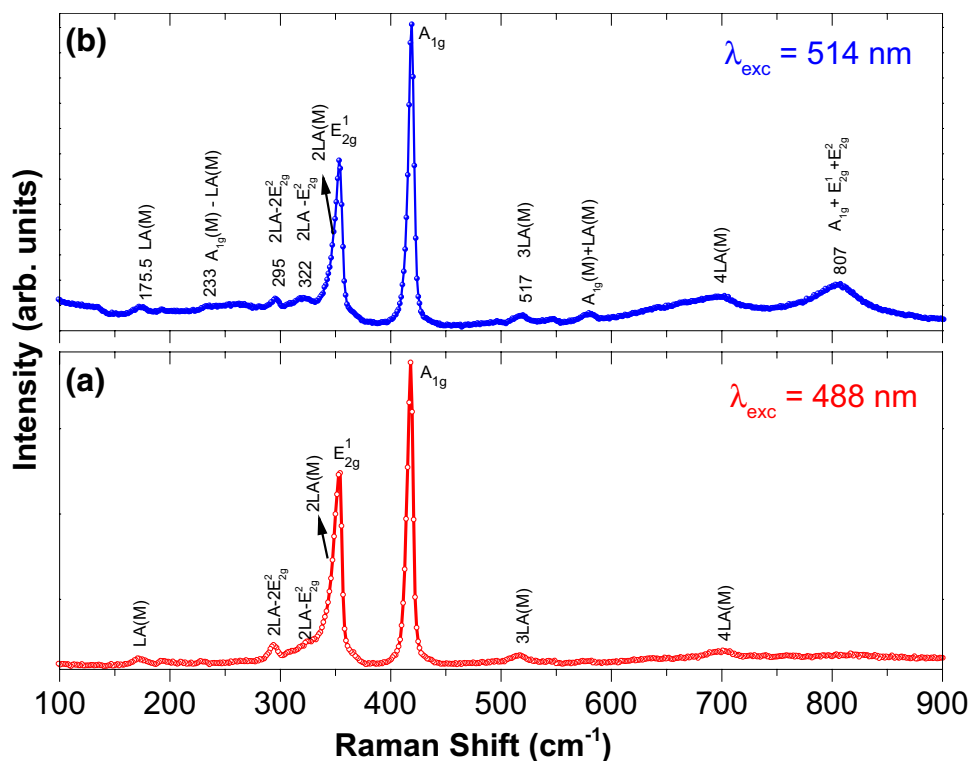
have shown that these two modes, i.e., A_{1g} (M) and A_{1g} (Σ) have dispersionless character in monolayer TMDCs [23, 24].

Figure 3 shows the typical linear absorption spectrum of WS_2 nanostructures acquired at room temperature. The absorption data is deconvoluted using gaussian function and we see that spectra consists of various spectral peaks at 627 nm, 523 nm, 458 nm, 395 nm and 327 nm together with a band edge absorption in the ultra voilet region. The first two peaks at 627 nm and 523 nm and are characteristics exciton peaks 'A' and 'B', respectively. These two peaks belong to the lowest energy exciton states and are due to transitions from the highest energy spin–orbit coupling induced split-off valence bands to the lowest energy conduction band states at the K point in the Brillouin zone [20, 25–27]. The energy separation between peaks A and B is close to 0.4 eV. This is in good agreement with the theoretically calculated and previously experimentally reported value for WS_2 [9, 26–28]. It should be noted that excitonic absorptions A and B are not due to quantum dots rather they corresponds to the few layered sheets of WS_2. Another absorption feature marked as C and the one at 458 nm is attributed to the transitions between density of states peaks between valence band and conduction bands [27]. The absorption spectra also reveal absorptions close to 395 nm (3.14 eV) and 327 nm (3.79 eV) together with band edge absorption in the ultraviolet region. The indirect band gap in bulk WS_2 is $\approx$ 1.2 eV [28] whereas the direct band gap in mono layer of WS_2 is around 2.1 eV. Recently, indirect transitions with energy larger than these values have been predicted in few-layer sheets of MoS_2 and WS_2 [29]. But the energy separation between corresponding valence band maxima and conduction band minima is much lower than the 395 nm and 327 nm absorptions we have noticed. In a recent study, Lin et al. have shown that WS_2 quantum dots with size in the range 8–15 nm possess a very large direct transition energies 3.16 eV (393 nm) and 3.73 eV (333 nm) compared to the WS_2 few layer sheets
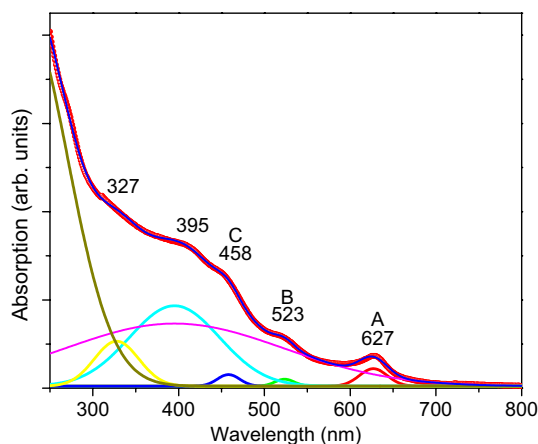
(2.1 eV). They have also shown that room temperature photoluminescence from such nanostructures is enhanced and lies in the blue-green spectral region [20]. Thus, it is very unlikely that in present samples the absorptions at 395 nm and 327 nm are linked with the absorption spectrum of few layer sheets of WS_2. The band edge absorption in the UV region is quiet far away from direct or indirect band gap in WS_2, it is indeed the absorption feature arising from the WS_2 quantum dots. These two peaks are likely to be the excitonic absorptions A and B from the quantum dots and are at relatively shorter wavelength than is the case for WS_2 few layered sheets (627 and 523 nm). The energy separation between two peaks (327 nm and 395 nm) is 650 meV (near IR region, $\approx$ 1907 nm), much larger than observed for few layer sheets (400 meV). These results, suggest that by rightly controlling the lateral size of the quantum dots, spin–orbit splitting in these nanostructures can be tuned. The next immediate question is that can we observe such a large enhancement in band gap when material is transformed from bulk into quantum dots. The Bohr radius determines the relevant particle size at which quantum confinement effects governing such enhancement in band gap are expected. For WS_2 the Bohr radius is around 3.7 nm. This implies that nanostructures with size in the range of $\approx$ 8 nm may give rise to larger band gap. Under effective mass approximation, the band gap variation with size is expressed through the following relationship [30].

$$E^* = E_g + \frac{h^2}{8\mu r^2} - \frac{1.8e^2}{4\pi\varepsilon_0\varepsilon_r} \qquad (1)$$

where, E_g is band gap of bulk material, r is radius of the quantum dot or nanoparticle, ε_0 is permittivity of free space and ε_r being relative permittivity of the material and $\mu = \frac{m_e m_h}{m_e + m_h}$ being reduced mass of the exciton. In case of WS_2 the effective mass of electron, m_e = 0.33 m_0 and that of hole m_h = 0.43 m_0 [31]. The quantum dots size in present sample ranges from 4 to 10 nm. Equation (1) predicts a band gap of 3.95–1.71 eV for particle with size ranging from 4 to 10 nm. Thus, such a large enhancement in band gap is expected and attributed to quantum confinement effects within WS_2 nanostructures. Further, it should be noted that possibility of nanostructures with size smaller than 4 nm cannot be excluded. Unlike other semiconductors, the absorption spectra for WS_2 does not display gap between various excitonic features and band edge absorption, thus elevating the problem of accurate determination of various peak positions. Further, difference in exact peak position might arise due to life time broadening and overlap with higher energy excitonic absorptions, excited states of excitons and/or electron–phonon coupling that results in continuous absorption [32, 33].

Fig. 3 UV–vis spectra of WS_2 nanostructures

Figure 4 shows the photoluminescence emission spectra acquired in the temperature range from 20 to 70 °C with $\lambda_{exc} = 310$ nm. As we see, the emission intensity reduces and the spectra also display a slight red-shift with rise in temperature. In Fig. 5 the emission spectra obtained at 20 °C is shown. The deconvolution of the spectra reveals three emission peaks at ≈ 340 nm, 390 nm and 432 nm. These three emission peaks corresponds to the absorption features noticed in the UV–visible measurements. The energy separation between former two peaks is ≈ 480 meV, larger than the value found in bulk WS_2 (≈ 400 meV). Lin et al. has attributed these features to the spin–orbit coupling induced splitting of valence band in confined WS_2 quantum dots [20]. Zhu et al. has recently demonstrated that due to broken inversion symmetry a giant spin splitting of the order of 456 meV is expected in monolayered WS_2 [34]. Due to inversion asymmetry in monolayer WS_2, the d-orbital corresponding to W atoms have strong spin-orbit coupling. As a result, largest splitting at K point of the Brillouin zone is observed. The expected enhancement in the band gap due to quantum confinement effect also suggests that corresponding excitonic features may appear at relatively higher energies in such nanostructures. Therefore, larger energy separation between two peaks at lower wavelength is justified in quantum confined WS_2 quantum dots. Further, Lin et al. also reported a large PL emission which is blue-shifted as compared with the emission from monolayered sheets. These, results suggest the role of quantum confinement effects in determining the optical properties of such 2-D nanostructures. Further, little red-shift in the PL spectra is similar to that observed in semiconductors. In semiconductors, the optical band gap reduces with rise in temperature, causing a red shift in absorption/emission spectra. This is widely accepted phenomena in semiconductors and is attributed to
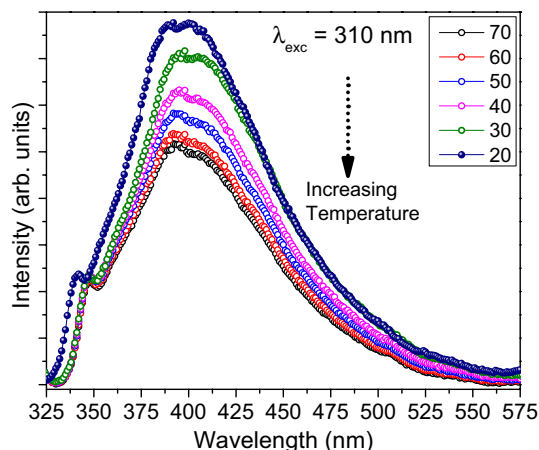

Fig. 5 Deconvoluted photoluminescence spectra of WS_2 nanostructures. The spectra were obtained at $\lambda_{exc} = 310$ nm

increased electron–phonon interaction and/or lattice expansion at higher temperature [16, 17].

To investigate other spectral features, the PL emission with $\lambda_{exc} = 400$ nm and in the temperature range 20–90 °C was also taken (Fig. 6). A closed analysis reveals four peaks at 445 nm, 468 nm, 495 nm and 534 nm. The emission feature at 445 nm might be similar to the one at 432 nm (obtained with $\lambda_{exc} = 310$ nm). Thus, we see that emission peaks are slightly shifted w.r.t the absorption spectra in Fig. 3. Further, with two different excitations, the PL spectra is different. This is a signature of slight polydisperse nature of the sample [9]. At lower excitation wavelength emission spectrum over wider energy range is obtained whereas at higher excitation wavelength the emission covers an energy range at higher wavelength. It is surprising that we did not observe the PL emission corresponding to absorption 'A'.

Figure 7a shows the variation of intensity with temperature for the emission peak at 390 nm. This peak corresponds

Fig. 4 Photoluminescence spectra of WS_2 nanostructures at different temperatures. Spectra were acquired with an excitation wavelength of 310 nm
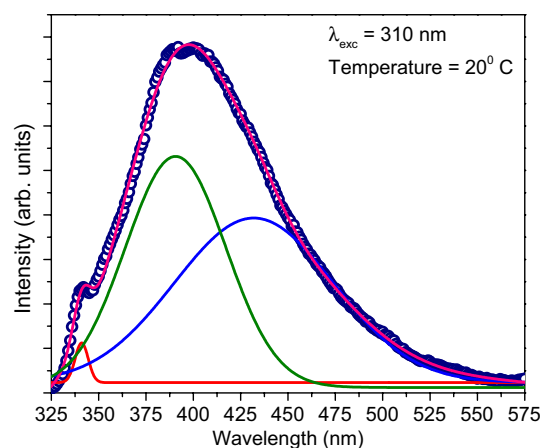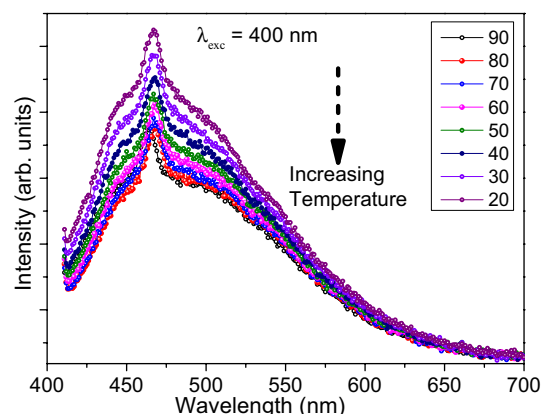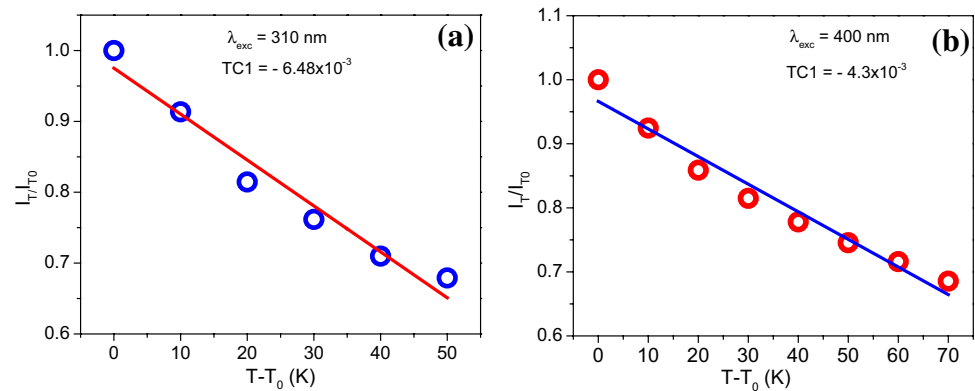

Fig. 6 Photoluminescence spectra of WS_2 nanostructures. The spectra were acquired at different temperatures with $\lambda_{exc} = 400$ nm

Fig. 7 Intensity variation with temperature. Data is given for PL spectra acquired at **a** $\lambda_{exc} = 310$ nm for PL emission corresponding to peak at 390 nm and **b** $\lambda_{exc} = 400$ nm for emission peak at 468 nm

to $\lambda_{exc} = 310$ nm. Similar data is shown in Fig. 7b for emission peak at 468 nm obtained with $\lambda_{exc} = 400$ nm. Here I_{T0} and and I_T are the emission intensities at 20 °C and any other temperature, respectively. In the former case the linear fit to the data gives the first order temperature coefficient $\approx -6.48 \times 10^{-3}$ K^{-1} whereas in latter case its value is -4.3×10^{-3} K^{-1}, relatively smaller than the value observed in previous case. The temperature dependent emission intensity is usually expressed as [8, 14, 35].

$$I(T) = \frac{I_{0\times} k_{rad}(T)}{k_{rad}(T) + k_{nonrad}(T)} \qquad (2)$$

where, I_0 is the maximum emission intensity at low temperature, $k_{rad}(T)$ and $k_{nonrad}(T)$ are the temperature dependent radiative and non-radiative recombination rates, respectively. The latter constitutes, the recombination rates due to trapping at defects sites and electron relaxation within the conduction band and valence bands. The intra-band relaxation to the band minima is usually accompanied with faster rates and may give rise to emission at lower energy compared to absorption peaks. Further, the increased electron–phonon interactions at higher temperature give rise to the thermally activated non-radiative recombination. As a result the emission intensity and hence the quantum efficiency decrease dramatically with increase in the temperature. In general the increased temperature causes a reduction in the band gap of a semiconductor, which is attributed to the enhanced electron–phonon interactions as well as lattice expansion at higher temperature [16, 17]. A qualitative idea about redshift can also be gained from the shift of other absorption feature. For instance, the absorption features at ≈ 327 nm appear at ≈ 340 nm in the emission spectra. Further, a redshift, although very small, is also visible from the emission spectra at different temperatures. The temperature dependence of emission intensity is fitted with the equation:

$$I_T = I_{T_0}[1 + \alpha(T - T_0)] \qquad (3)$$

where, I_T and I_{T0} are the emission intensities at temperature T and reference temperature (20 °C), respectively and α is the first order temperature coefficient. The fit to the emission data is shown in Fig. 7a, b. Negative α values, 6.48×10^{-3} K^{-1} and 4.3×10^{-3} K^{-1} have been obtained for the emission intensity corresponding to peaks at 390 nm ($\lambda_{exc} = 310$ nm) and 468 nm ($\lambda_{exc} = 400$ nm).

4 Conclusions

We have measured systematically the room temperature Raman spectra and the temperature-dependent photoluminescence spectra of few layer sheets and quantum dots of WS_2. The resonance Raman spectra with 514 nm excitation revealed various higher order modes which were inaccessible with other excitation. The nanostructures display various excitonic features corresponding to a few layer WS_2 and a band edge absorption in the ultraviolet region. We observed that the photoluminescence intensities of the WS_2 nanostructures decrease with rise in temperature. This is attributed to the increased electron–phonon interactions at higher temperature. A slight red-shift in the photoluminescence emission with rise in temperature is also noticed. Such red-shift might arise from the anharmonic effects. Further, the optical studies revealed that WS_2 quantum dots exhibits absorptions at much smaller wavelengths with larger spin–orbit coupling ≈ 650 meV, larger than observed for monolayer sheets of WS_2 (≈ 400 meV). This is in agreement with the quantum confinement effects in these nanostructures and previously observed values for WS_2 quantum dots. These results indicates indicate that by rightly controlling the dimensions of the nanostructures the strength of spin–orbit splitting can be tuned and hence a control over optical properties can be achieved.

References

1. Q.H. Wang, K.K. Zadeh, A. Kis, J.N. Coleman, M.S. Strano, Electronics and optoelectronics of two-dimensional transition-metal dichalcogenides. Nat. Nanotechnol. **7**, 699–712 (2012)

2. K.S. Novoselov, Graphene: materials in the flatland (Nobel lecture). Angew. Chem. Int. Ed. **83**, 837–849 (2011)

3. K.S. Novoselov, D. Jiang, F. Schedin, T.J. Booth, V.V. Khotkevich, S.V. Morozov, A.K. Geim (2005) Two-dimensional atomic crystals. Proc Natl Acad Sci USA 102:3010451–3010453

4. B.K. Miremadi, S.R. Morrison, The intercalation and exfoliation of tungsten disulfide. J. Appl. Phys. **63**, 4970 (1988)

5. A. Ghorai, A. Midya, R. Maiti, S.K. Ray, Exfoliation of WS_2 in the semiconducting phase using a group of lithium halides: a new method of Li intercalation. Dalton Trans. **45**, 14979–14987 (2016)

6. J.P. Wilcoxon, G.A. Samara, Strong quantum-size effects in a layered semiconductor: MoS_2 nanoclusters. Phys. Rev. B **51**, 7299–7302 (1995)

7. D.H. Feng, Z.Z. Xu, T.Q. Jia, X.X. Li, S.Q. Gong, Quantum size effects on exciton states in indirect-gap quantum dots. Phys. Rev. B **68**, 035334 (2003)

8. A. Splendiani, L. Sun, Y. Zhang, T. Li, J. Kim, C.Y. Jonghwan Chim, G. Galli, F. Wang, Emerging photoluminescence in monolayer MoS_2. Nano Lett. **10**, 1271–1275 (2010)

9. S. Sharma, S. Bhagat, J. Singh, R.C. Singh, S. Sharma, Excitation-dependent photoluminescence from WS_2 nanostructures synthesized via top-down approach. J. Mater. Sci. **52**, 11326–11336 (2017)

10. S. Bhagat, S. Sharma, J. Singh, S. Sharma, Strain-induced tuning of optical properties of layered MoS_2 in communication

11. S. Bhattacharyya, T. Pandey, A.K. Singh, Effect of strain on electronic and thermoelectric properties of few layers to bulk MoS_2. Nanotechnology **25**, 465701 (2014)

12. H. Keliang, P. Charles, M.K. Fai, S. Jie, Experimental demonstration of continuous electronic structure tuning via strain in atomically thin MoS_2. Nano Lett. **13**, 2931–2936 (2013)

13. H. Yeung Yu, L. Xiaofei, J. Wenjing, C.N. Chan Yui, H. Jianhua, H. Yu-Te, L. Lain-Jong, G. Wanlin, L.S. Ping, Exceptional tunability of band energy in a compressively strained trilayer MoS2 sheet. ACS Nano **7**, 7126–7131 (2013)

14. Y. Chen, W. Wen, Y. Zhu, N. Mao, Q. Feng, M. Zhang, H.P. Hsu, J. Zhang, Y.S. Huang, L. Xie, Temperature-dependent photoluminescence emission and Raman scattering from $Mo_{1-x}W_xS_2$ monolayers. Nanotechnology **27**, 445705 (2016)

15. S.M. Sze, N.K. Kwok. (2006) Physics and Properties of Semiconductors A Review. Wiley, New York, pp 5–75

16. Y.P. Varshni, Temperature dependence of the energy gap in semiconductors. Physica **34**, 12170–12177 (1967)

17. K.P.O. Donnell, X. Chen, Temperature dependence of semiconductor band gaps. Appl. Phys. Lett. **58**, 2924–2926 (1991)

18. J. Pandey, A. Soni, Unraveling biexciton and excitonic excited states from defect bound states in monolayer MoS_2. Appl. Surf. Sci. **463**, 52–57 (2019)

19. S. Sharma, J. Singh, S. Bhagat, M. Singh, S. Sharma, Size tunable photoluminescence from WS2 nanostructures. Mater Res Express **5**, 045047 (2018)

20. L. Liangxu, X. Yaoxian, Z. Shaowei, R.M. Ian, C.M. Ong Albert, D.A. Allwood, Fabrication of luminescent monolayered tungsten dichalcogenides quantum dots with giant spin-valley coupling. ACS Nano **7**, 8214–8223 (2013)

21. A. Berkdemir, H.R. Gutierrez, A.R. Botello-Mendez et al., Identification of individual and few layers of WS_2 using Raman spectroscopy. Sci. Rep. **3**, 1755- (2013)

22. X. Zhang, Q. Xiao-Fen, S. Wei, W. Jiang-Bin, J. De-Sheng, T.P. Heng, Phonon and Raman scattering of two-dimensional transition metal dichalcogenides from monolayer, multilayer to bulk material. Chem. Soc. Rev. **44**, 2757–2785 (2015)

23. N. Wakabayashi, H.G. Smith, R.M. Nicklow, Lattice dynamics of hexagonal MoS_2 studied by neutron scattering. Phys. Rev. B **12**, 659–663 (1975)

24. A. Molina, L. Wirtz, Phonons in single-layer and few-layer MoS_2 and WS_2. Phys. Rev. B **84**, 155413 (2011)

25. H.M. Hill, A.F. Rigosi, C. Roquelet, A. Chernikov, T.C. Berkelbach, D.R. Reichman, M.S. Hybertsen, L.E. Brus, T.F. Heinz, F. Tony, Observation of excitonic rydberg states in monolayer MoS_2 and WS_2 by photoluminescence excitation spectroscopy. Nano Lett. **15**, 992–2997 (2015)

26. A. Ramasubramaniam, Large excitonic effects in monolayers of molybdenum and tungsten dichalcogenides. Phys. Rev. B **86**, 115409 (2012)

27. W. Zhao, Z. Ghorannevis, L. Chu, M. Toh, C. Kloc, P.H. Tan, G. Eda, Evolution of electronic structure in atomically thin sheets of WS_2 and WSe_2. ACS Nano **7**, 791–797 (2013)

28. R.A. Bromley, R.B. Murray, A.D. Yoffe, The band structures of some transition metal dichalcogenides. III. Group VIA: trigonal prism materials. J. Phys. C Solid State Phys. **5**, 759 (1972)

29. W. Zhao, R.M. Ribeiro, M. Toh, A. Carvalho, C. Kloc, A.H.C. Neto, G. Eda, Origin of indirect optical transitions in few-layer MoS_2, WS_2, and WSe_2. Nano Lett. **13**, 5627–5634 (2013)

30. Z.X. Gan, L.Z. Liu, H.Y. Wu, Y.L. Hao, Y. Shan, X.L. Wu, P.K. Chu, Quantum confinement effects across two-dimensional planes in MoS_2 quantum dots. Appl. Phys. Lett. **106**, 233113 (2015)

31. J. Chang, L.F. Register, S.K. Banerjee, Ballistic performance comparison of monolayer transition metal dichalcogenide MX_2(M = Mo, W; X = S, Se, Te) metal-oxide-semiconductor field effect transistors. J. Appl.**Phys. 115**, 084506 (2014)

32. D.Y. Qiu, F.H. da Jornada, S.G. Louie, Optical spectrum of MoS_2: Many-body effects and diversity of exciton states. Phys. Rev. Lett. **111**, 216805 (2013)

33. K. He, N. Kumar, L. Zhao, Z. Wang, K.F. Mak, H. Zhao, J. Shan, Tightly bound excitons in monolayer WSe_2. Phys. Rev. Lett. **113**, 026803 (2014)

34. Z.Y. Zhu, Y.C. Cheng, U. Schwingenschlogl, Giant spin-orbit-induced spin splitting in two-dimensional transitional-metal dichalcogenide semiconductors. Phys. Rev. B **84**, 153402 (2011)

35. N. Haiyan, W. Zilu, W. Wenhui, L. Zheng, L. Yan, C. Qian, H. Daowei, T. Pingheng, M. Feng, W. Xinran, W. Jinlan, N. Zhenhua, Strong photoluminescence enhancement of MoS_2 through defect engineering and oxygen bonding. ACS Nano **8**, 5738–5745 (2014)